THE JOURNAL OF PHYSICAL CHEMISTRY LETTERS
A JOURNAL OF THE AMERICAN CHEMICAL SOCIETY

pubs.acs.org/JPCL
Letter

Operando Evaluation of the Electrochemically Active Area in a Solid Oxide Fuel Cell Porous Electrode by Micro X-ray Absorption Spectroscopy

Yoshinobu Fujimaki, Takashi Nakamura, Yuta Kimura, Kiyofumi Nitta, Oki Sekizawa, Yasuko Terada, Keiji Yashiro, Tatsuya Kawada, and Koji Amezawa*

Cite This: J. Phys. Chem. Lett. 2025, 16, 9599−9605

Read Online

ACCESS | Metrics & More | Article Recommendations | Supporting Information

ABSTRACT: An operando X-ray absorption spectroscopic technique, which enables us to measure X-ray absorption spectra with a position resolution of submicrometers at increased temperatures while controlling atmospheres and passing an electrical current through the specimen, was developed. By applying this technique, the electrochemically active area in a porous $La_{0.6}Sr_{0.4}CoO_{3-\delta}$ electrode for a solid oxide fuel cell (SOFC) was experimentally and directly evaluated for the first time. The characteristic length of the active area was approximately 1 μm from the electrode−electrolyte interface under a cathodic overpotential of 140 mV at 873 K under 10^{-2} bar of $P(O_2)$, although the investigated electrode was thicker than 50 μm. This demonstrated that a reaction in an SOFC electrode inhomogeneously proceeds in a very limited area near the electrode−electrolyte interface, even when a mixed ionic and electronic conducting oxide is used as the electrode, and that direct evaluation of the active area can provide guidelines for high-performance electrode design.

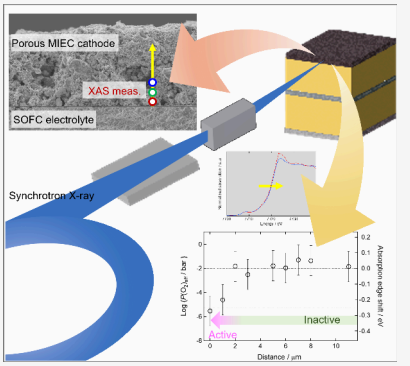

The solid oxide fuel cell (SOFC) is one of the promising candidates for next-generation environmentally friendly power sources for a sustainable society because of its high efficiency and fuel flexibility.[1−4] SOFCs are typically operated around 973−1273 K, and such high-temperature operation causes several practical issues in terms of long-term reliability and durability. Decreasing the operating temperature is one solution for these issues, and hence, intermediate-temperature SOFCs have recently attracted much attention. However, decreasing the operating temperature results in serious performance degradation, especially in the cathode. In order to establish high-performance cathodes working at intermediate temperatures, we must understand the factors that govern the electrode reaction.

Mixed ionic and electronic conductors (MIECs), for instance, $(La,Sr)(Co,Fe)O_{3-\delta}$, are currently utilized as SOFC cathode materials.[2,3] In an MIEC cathode, the electrochemical reaction can proceed not only at the triple-phase boundaries (gas−electrode−electrolyte) but also at the double-phase boundaries (gas−electrode). Possible elemental reaction steps in the MIEC cathode are considered as follows: (i) oxygen adsorption and dissociation on the electrode surface, (ii) ionization of the oxygen atom and incorporation into the electrode bulk, (iii) oxide ion diffusion in the electrode bulk, and (iv) oxide ion transfer from the electrode bulk into the electrolyte bulk. The rates of steps i and ii are described by surface exchange coefficient k, and that of the step iii is described by diffusion coefficient D. Since the resistance for oxide ion diffusion in an MIEC SOFC electrode increases with the distance from the electrode−electrolyte interface, the electrochemical reaction does not proceed homogeneously in the whole area of the practical porous electrode. The reaction current is considered to decrease with an increase in the distance from the interface. Therefore, to improve the electrode performance, it is important to understand how the reaction is distributed in the electrode and to optimize the electrode materials and microstructures.

Adler et al. theoretically discussed such an inhomogeneous reaction in a porous MIEC SOFC electrode.[5] Based on their model, the so-called Adler−Lane−Steele (ALS) model, they simulated the profiles of the reaction current in a porous MIEC SOFC electrode under polarization and showed that the reaction distribution can be principally determined by the competition between the resistances for the surface reaction and oxide ion diffusion.[5,6] The electrochemically active area is predicted to increase when the resistance is larger for the surface reaction or smaller for oxide ion diffusion. The resistances for the surface reaction and oxide ion diffusion can

Received: August 5, 2025
Revised: August 28, 2025
Accepted: August 29, 2025
Published: September 6, 2025

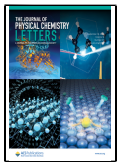

https://doi.org/10.1021/acs.jpclett.5c02422
J. Phys. Chem. Lett. 2025, 16, 9599−9605

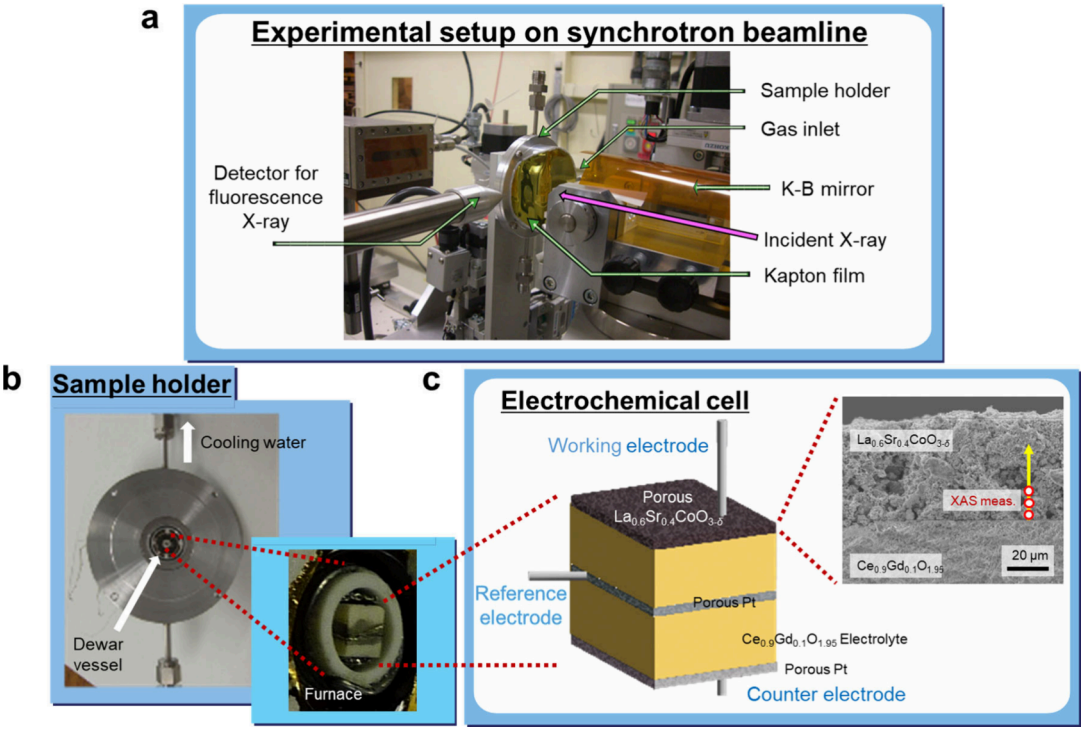

Figure 1. Experimental setup for operando high-tempearature electrochemical micro X-ray absorption spectroscopy measurements. (a) Overview of experimental setup on the synchrotron beamline. (b) Three-terminal electrochemical cells mounted on a sample holder. (c) Schematic illustration of the electrochemical cell and cross-sectional SEM image of the porous $La_{0.6}Sr_{0.4}CoO_{3-\delta}$ electrode investigated.

be determined by surface exchange coefficient k and diffusion coefficient D of the electrode material, respectively, if the electrode microstructures, such as tortuosity, particle size, surface area, and porosity, are known. Based on this idea, the electrochemically active area has been evaluated from k and D values.[5−15] For instance, Lu et al. calculated the electrochemically active area in porous $La_{0.6}Sr_{0.4}CoO_{3-\delta}$ by using k and D values obtained from electrochemical impedance spectroscopy (EIS) measurement.[5] By combining 3D reconstruction of the electrode microstructures and calculation by the finite element method (FEM) model while using k and D values from the literature, Carraro et al. have presented the electrochemically active area in a porous $La_{0.58}Sr_{0.4}Co_{0.2}Fe_{0.8}O_{3-\delta}$ electrode.[8] Recently, attempts to predict the performance and the reaction distribution of SOFC electrodes were made using machine learning of the electrode microstructures, although the target was not MIEC but cermet fuel electrodes.[16] There is no doubt that these evaluations are well-conceived for the examination of the distribution of the electrochemical reaction in SOFC electrodes. However, it is true that these are not direct observations, and no one could ensure the validity of the evaluations.

Considering the background mentioned above, in this work, we aimed to establish a methodology for the direct evaluation of the reaction distribution in an MIEC SOFC electrode near the infterce with an electrolyte. For this purpose, we developed operando high-temperature electrochemical micro X-ray absorption spectroscopy (XAS). This technique enables us to measure X-ray absorption spectra with a positional resolution higher than 1 μm, while controlling temperature and atmospheric conditions, and passing an electrical current through the electrode. Then, this operando local analytical technique was applied to investigate the reaction distribution in a porous $La_{0.6}Sr_{0.4}CoO_{3-\delta}$ electrode on a $Ce_{0.9}Gd_{0.1}O_{1.95}$ electrolyte, which are a typical MIEC cathode and oxide ion-conducting electrolyte for SOFC, respectively. To the best of our knowledge, this is the first report that directly evaluated the reaction distribution in a practical porous SOFC electrode in an experimental manner.

X-ray absorption spectroscopy can give us information about the electronic and chemical states of the material investigated. For instance, in $La_{0.6}Sr_{0.4}CoO_{3-\delta}$ investigated in this study, it was reported that the mean oxidation state of the Co ion can be estimated from the shift of the absorption-edge energy in the Co K-edge XAS spectrum.[17,18] According to our previous operando XAS measurements using a dense thin film of $La_{0.6}Sr_{0.4}CoO_{3-\delta}$ as the model electrode, we demonstrated that cathodic polarization partially reduces the electrode oxide even when the ambient $P(O_2)$ is constant.[19] It was also shown that the electrode is reduced more as a larger electrode overpotential is applied, i.e., a larger reaction current is passed.[19] Such "electrochemical reduction" suggested that the oxygen chemical potential is effectively decreased at the electrode surface due to cathodic polarization, because the surface reaction is the rate-determining elementary step in the case of electrochemical oxygen reduction on $La_{0.6}Sr_{0.4}CoO_{3-\delta}$.[20,21] These findings tell us that the oxygen chemical potential changes depending on the amount of reaction current and therefore that the reaction distribution in the electrode can be directly clarified if the distribution of oxygen chemical potential is detected. In this study, by applying the developed operando high-temperature electrochemical micro XAS technique, the oxygen chemical potential at the desired position in a porous $La_{0.6}Sr_{0.4}CoO_{3-\delta}$ electrode was evaluated by detecting the change in the mean oxidation state of the Co ion. By repeating this measurement under constant cathodic

https://doi.org/10.1021/acs.jpclett.5c02422
J. Phys. Chem. Lett. 2025, 16, 9599−9605

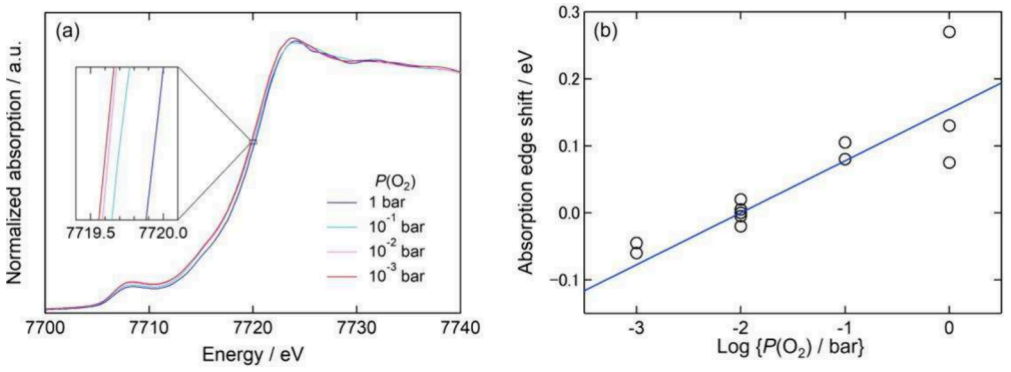

Figure 2. Co K-edge X-ray absorption spectroscopy measurements of $La_{0.6}Sr_{0.4}CoO_{3-\delta}$ at 873 K. (a) XANES spectra at various ambient oxygen partial pressures $P(O_2)$ under an open circuit. (b) Shift of the absorption-edge energy as a function of $P(O_2)$.

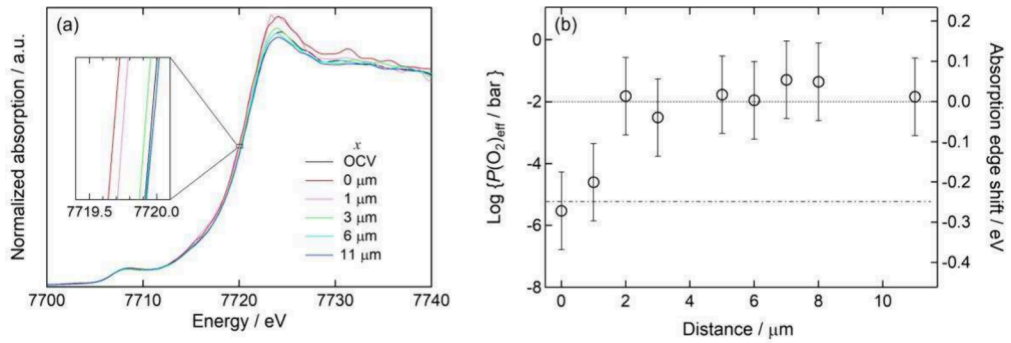

Figure 3. Operando Co K-edge X-ray absorption spectroscopy measurements of the porous $La_{0.6}Sr_{0.4}CoO_{3-\delta}$ electrode at 873 K, a $P(O_2)$ of 10^{-2} bar, and a cathodic overpotential of 140 mV. (a) Co K-edge XANES spectra observed at various positions in the electrode. (b) Distibution of effective oxygen partial pressure $P(O_2)_{eff}$ as a function of the distance from the electrode−electrolyte interface.

polarization while changing the measuring point, we clarified the reaction distribution in the practical porous electrode as a function of the distance from the electrode−electrolyte interface.

In order to directly evaluate the reaction distribution in an MIEC SOFC electrode, an analysis technique that can analyze the electronic and chemical states of the electrode with sufficiently high positional resolution is required. In addition, the analysis should be carried out under SOFC operating conditions, namely, at increased temperatures in a controlled atmosphere while passing an electrical current through a specimen. With such an analytical technique, operando high-temperature electrochemical micro XAS was developed in this study. For XAS measurements with high positional resolution, the incident X-ray beam was focused into a 0.5 μm × 0.8 μm area by using a Kirkpatrick-Baez mirror. A three-terminal electrochemical cell was prepared and mounted atop an electric furnace in the sample holder for operando XAS measurements.[18,22] Pictures of the experimental setup at the synchrotron beamline and the electrochemical cell on the sample holder are shown in Figure 1. The cross section of the cell was placed face up, as shown in the bottom left picture and bottom right schematic illustration of Figure 1. The focused X-ray was incident perpendicular to the cross section of the cell, so that the electronic and chemical states of the electrode material can be analyzed in the electrode thickness direction as a function of the distance from the electrode−electrolyte interface. XAS measurements were carried out in fluorescence mode. Since the attenuation length of the X-ray with the energy around the Co K-edge is calculated as 5 μm in $La_{0.6}Sr0.4CoO_{3-\delta}$, the observed signal of the fluorescence X-ray is thought to reflect the average electronic structure of the electrode within this length from the observation surface (the electrode cross section) in the direction of the incident X-ray. The measuring positions were determined based on the result of 2D elementary mapping by fluorescence X-ray analysis of Co Kα (electrode) and Ce Lα (electrolyte). The sample holder was covered by an Al-coated Kapton film, and the atmosphere inside the holder was kept constant by a gas flow. By using these setups, an X-ray absorption spectrum could be measured with a positional resolution higher than 1 μm at the desired position under controlled temperature, atmosphere, and polarization.

As mentioned in the beginning of this section, it is known that the Co K-edge absorption energy of $La_{0.6}Sr_{0.4}CoO_{3-\delta}$ is shifted depending on the oxygen chemical potential (oxygen partial pressure) to which the material is exposed. This happens because the increase or decrease in oxygen chemical potential causes a decrease or increase, respectively, in oxygen vacancy concentration δ and consequently a decrease or increase, respectively, in the mean valence of the Co ion in $La_{0.6}Sr_{0.4}CoO_{3-\delta}$. This indicates that the change in the oxygen chemical potential in $La_{0.6}Sr_{0.4}CoO_{3-\delta}$ can be evaluated by measuring the Co K-edge X-ray absorption spectra if the temperature is kept constant. In this work, for the purpose of evaluating the change in the oxygen chemical potential or effective oxygen partial pressure $P(O_2)_{eff}$, due to polarization, the Co K-edge X-ray absorption spectra of the porous $La_{0.6}Sr_{0.4}CoO_{3-\delta}$ electrode were first measured at various ambient $P(O_2)$ values under open circuit conditions at a constant temperature of 873 K, and then the calibration line, correlating the Co K-edge absorption energy with $P(O_2)_{eff}$, was

https://doi.org/10.1021/acs.jpclett.5c02422
J. Phys. Chem. Lett. 2025, 16, 9599−9605

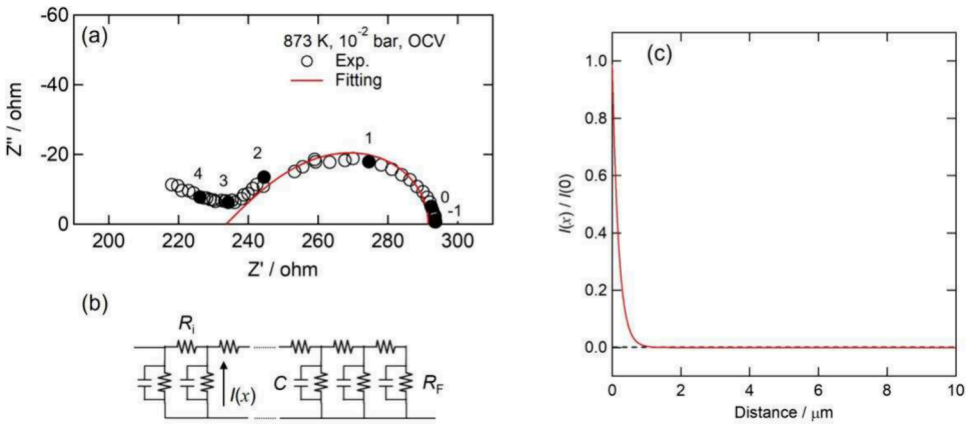

Figure 4. AC electrochemical impedance measurements of the porous $La_{0.6}Sr_{0.4}CoO_{3-\delta}$ electrode at 873 K and a $P(O_2)$ of 10^{-2} bar under open circuit conditions. (a) Nyquist plot and fitting curve by a semifinite transmission line model. The numbers in the figure represent the order of frequency. (b) Semifinite transmission line model used for the fitting. (c) Calculated distibution of the normalized Faradaic current as a function of the distance from the electrode−electrolyte interface.

obtained. In this series of measurements, the measuring position was fixed in the middle of the porous electrode.

Figure 2a shows the obtained Co K-edge X-ray absorption near-edge structure (XANES) spectra of the porous $La_{0.6}Sr_{0.4}CoO_{3-\delta}$ electrode under $1-10^{-3}$ bar of $P(O_2)$ under open circuit conditions at 873 K. The inset of Figure 2a shows a magnified view of the spectra near the absorption edge. The absorption energy was slightly decreased with ambient $P(O_2)$. A similar trend was found by ex situ measurements of the quenched samples in our previous papers.[17,18] Figure 2b shows the shifts of the Co K-edge absorption energy as a function of ambient $P(O_2)$. Here, the absorption-edge energy was defined as the energy at which half of the absorbance change of the XANES spectrum was observed and that under 10^{-2} bar of $P(O_2)$ was taken as the reference state. As shown in Figure 2b, the absorption energy seemed to linearly decrease with ambient $P(O_2)$. The amount of energy shift was approximately 0.22 eV between 1 and 10^{-3} bar of $P(O_2)$ at 873 K. An approximately straight line calculated by the least-squares method is shown as a solid line in Figure 2b. By using this line as a calibration line, the change in $P(O_2)_{eff}$ due to polarization can be quantitatively estimated from Co K-edge XAS measurements.

For the direct evaluation of the electrochemically active area, operando high-temperature electrochemical micro XAS measurements were carried out at the desired micro area in the porous $La_{0.6}Sr_{0.4}CoO_{3-\delta}$ electrode under cathodic polarization. Figure 3a shows the Co K-edge XANES spectra observed at various measuring positions under a constant cathodic overpotential of 140 mV and 873 K under 10^{-2} bar of $P(O_2)$. The experimental conditions were determined based on the practical operating conditions of the SOFC cathode and the ease of detecting the electrochemically active area by operando XAS measurement. In this figure, the spectrum observed under open circuit conditions is shown as the black curve for comparison. The position of the electrode−electrolyte interface was defined as a reference point, i.e., x = 0 μm. As shown in Figure 3a, the Co K-edge absorption energy was decreased at the positions near the electrode−electrolyte interface in spite of the constant ambient $P(O_2)$. The shift was gradually relaxed with an increase in the distance from the interface. At the positions far from the interface, the absorption energy was almost equivalent to that observed under open circuit conditions. These results suggested that, under cathodic polarization, (i) $P(O_2)_{eff}$ decreased near the electrode−electrolyte interface in the porous electrode even though the ambient $P(O_2)$ was kept constant and (ii) such a reducing condition due to cathodic polarization gradually relaxed with the distance from the electrode−electrolyte interface.

The $P(O_2)_{eff}$ under cathodic polarization at each measuring position was evaluated from the shift of the absorption-edge energy in the observed XANES spectra by using the calibration line in Figure 2b. Figure 3b gives $P(O_2)_{eff}$ as a function of the distance from the electrode−electrolyte interface. The dashed line in Figure 3b expresses the atmospheric $P(O_2)$, i.e., 10^{-2} bar. On the other hand, the dashed−dotted line gives the effective oxygen partial pressure at the electrode−electrolyte interface, $P(O_2)_{eff,int}$, which is expected from the applied cathodic overpotential. The relation between $P(O_2)_{eff,int}$ and applied overpotential η is described by the equation[20]

$$P(O_2)_{eff,int} = P(O_2)\exp\left(\frac{4F\eta}{RT}\right) \quad (1)$$

where $P(O_2)$ is the ambient oxygen partial pressure and F, R, and T are Faraday's constant, the gas constant, and the absolute temperature, respectively. As shown in Figure 3b, $P(O_2)_{eff}$ drastically decreased in the vicinity of the electrode−electrolyte interface. $P(O_2)_{eff}$ at the interface evaluated from the operando micro XAS measurement was comparable to $P(O_2)_{eff,int}$ predicted from eq 1. $P(O_2)_{eff}$ gradually increased with the distance from the interface. In the area approximately 2 μm from the interface, $P(O_2)_{eff}$ became comparable to ambient $P(O_2)$.

As previously mentioned, under cathodic polarization, a decrease in the oxygen chemical potential is expected in the area where the electrode reaction takes place. The size of the decrease in the oxygen chemical potential, which corresponds to the decrease in $\log\{(P(O_2)_{eff})\}$, reflects the amount of reaction current. Therefore, the result in Figure 3b demonstrates that the electrochemical reaction proceeded only within approximately 2 μm of the electrode−electrolyte interface in the porous $La_{0.6}Sr_{0.4}CoO_{3-\delta}$ electrode under a cathodic overpotential of 140 mV at 873 K in 10^{-2} bar of $P(O_2)$, although the electrode thickness was about 50 μm. In other words, only a very limited area in the electrode functions as the reaction sites even in a mixed ionic and electronic

https://doi.org/10.1021/acs.jpclett.5c02422
J. Phys. Chem. Lett. 2025, 16, 9599−9605

conducting electrode. This indicated that the thickness of the SOFC cathode can be made thinner than that in conventional SOFCs, although decreasing the electrode thickness may increase the resistance of the current collection in the in-plane direction of the electrode. To the best of our knowledge, this is the first study to directly and quantitatively observe the electrochemically active area in a practical SOFC porous electrode in an experimental manner. It is here noted that the length of the electrochemically active area possibly depends on the operating conditions (the magnitude of the overpotential, ambient $P(O_2)$, temperature, etc.) as well as electrode microstructures (porosity, specific surface area, tortuosity, etc.).

Adler et al. introduced the characteristic length, l_δ, that characterizes the distance of the electrochemically active area from the electrode−electrolyte interface in a porous MIEC electrode.[5−8] l_δ is defined as the distance between the electrode−electrolyte interface and the position where the amount of ionic current reaches $1/e$ of its maximum value at the interface. Considering Ohm's law, the overpotential, or the oxygen chemical potential, at distance l_δ is also $1/e$ of that at the interface. Following this definition, the characteristic length of electrochemically active area l_δ in the porous $La_{0.6}Sr_{0.4}CoO_{3-\delta}$ electrode in this study was 1 μm or less.

The electrochemically active area in MIEC SOFC electrodes has been extensively investigated by electrochemical measurements and numerical calculations. These are indirect but practically convenient ways to estimate the electrochemically active area. Figure 4a presents a typical AC EIS of the porous $La_{0.6}Sr_{0.4}CoO_{3-\delta}$ electrode in this work, which was taken under an open circuit at 873 K in 10^{-2} bar of $P(O_2)$. A Gerischer-type impedance response was observed. The electrode reaction in an MIEC SOFC porous electrode is often described by a semi-infinite transmission line model, as shown in Figure 4b. For this configuration, impedance $Z(\omega)$ is given by[23,24]

$$Z(\omega) = \sqrt{\frac{R_i}{\frac{1}{R_F} + j\omega C}} \tag{2}$$

where R_F and C are the resistance and the capacitance attributed to the electrode reaction, respectively, and R_i is the resistance of ionic transport in the electrode bulk. Then the reaction distribution, i.e., the Faradaic current as a function of the distance from the electrode−electrolyte interface, $I(x)$, is expressed by

$$I(x) = I(0)\exp\left[-\sqrt{\left(\frac{1}{R_F} + j\omega C\right)R_i}\,x\right] \tag{3}$$

Since l_δ is the distance between the electrode−electrolyte interface and the position where the amount of Faradaic current is $I(0)/e$ under DC polarization ($\omega = 0$), l_δ is described by R_F and R_i

$$l_\delta = \sqrt{\frac{R_F}{R_i}} \tag{4}$$

Considering eqs 2−4, the reaction distribution can be estimated if the values of R_F and R_i are obtained from the fitting of the impedance spectrum by the transmission line model. The solid curve in Figure 4a presents the fitting result when assuming the transmission line model, and Figure 4c shows the reaction distribution estimated from the obtained R_F and R_i. This distribution estimated from EIS is slightly precipitous compared with one directly observed by operando micro XAS, but it is reasonably similar in terms of the order of magnitude. Here it should be noted that l_δ values obtained from micro XAS and EIS measurements are different spatial information. l_δ obtained from micro XAS measurements is the local l_δ at the observed position. On the other hand, l_δ obtained from EIS measurements is the average l_δ across the entire electrode. Since microstructures of the porous electrode are complicated and not uniform depending on position, slightly different values of l_δ were thought to be obtained from micro XAS and EIS measurements.

Lu et al. reported a similar estimation of the electrochemically active area from EIS measurements for a porous $La_{0.6}Sr_{0.4}CoO_{3-\delta}$ electrode.[9] They estimated l_δ as approximately 1 μm at 923 K under 10^{-2} bar of $P(O_2)$. This value is close to that in this work, confirming the validity of our results, although we cannot simply compare the results because the measurement conditions and the electrode microstructures are slightly different.

According to the theoretical treatment by Adler et al.,[5−9] i.e., the ALS model, in the case of a mixed-conducting oxide like $La_{0.6}Sr_{0.4}CoO_{3-\delta}$, resistances R_F and R_i can be related to surface exchange coefficient k and diffusion coefficient D of the electrode material, respectively, if the electrode microstructures, such as porosity, specific surface area, and tortuosity, are known. On the other hand, capacitance C can be related to the thermodynamic factor for the oxygen nonstoichiometric change of the electrode material. As a result, it was shown that the electrochemically active area can be determined by the ratio between the diffusion coefficient and the surface exchange coefficient (D/k) when the electrode material and microstructures are the same. Based on this treatment, Carraro et al. numerically discussed the reaction distribution while including the real 3D electrode microstructures constructed by FIB-SEM analysis in the calculation.[12,13] They simulated the dimensionless reaction current profile in a porous $La_{0.58}Sr_{0.4}Co_{0.2}Fe_{0.8}O_{3-\delta}$ electrode by using literature values of k and D and then obtained l_δ within 1 μm at 873 K in air. A similar three-dimensional numerical analysis was also performed by Matsuzaki et al., and l_δ in a porous $La_{0.6}Sr_{0.4}Co_{0.2}Fe_{0.8}O_{3-\delta}$ electrode was reported as 5 μm at 973 K in 0.20 bar of $P(O_2)$.[15] Again, we cannot simply compare these results with ours, because the electrode materials, electrode microstructures, and experimental conditions were different. However, if l_δ is proportional to the square root of D/k as Adler et al. suggested,[5−9] l_δ is presumed to increase with a decrease in $P(O_2)$ while insignificantly depending on overpotential and temperature. Assuming such changes in l_δ depending on the experimental conditions, the values of l_δ reported above reasonably agree with our results from XAS measurements in this study. These facts verify the theory that the electrochemically active area can be principally determined by k and D.

As discussed throughout this paper, we succeeded in establishing an experimental technique for the direct evaluation of the reaction distribution in an MIEC SOFC electrode. However, as shown in Figure 3b, the experimental error in $P(O_2)_{eff}$ estimated from XANES spectra is relatively large. Such a large experimental error is considered to arise mainly from the inhomogeneity of the electrode microstructure. Microstructures of a porous electrode are complicated and not uniform from position to position. Thus, the reaction

https://doi.org/10.1021/acs.jpclett.5c02422
J. Phys. Chem. Lett. 2025, 16, 9599−9605

distribution cannot be expressed simply only as a function of the distance from the electrode−electrolyte interface in the case of a porous electrode.[14,15] On the other hand, the operando micro XAS technique developed in this work gives us the average $P(O_2)_{eff}$ in the direction of the incident X-ray, although it has a high position resolution in the in-plane direction perpendicular to the X-ray incident direction. To clarify the influence of the electrode microstructures on the reaction distribution, it would be effective to perform operando micro XAS measurements and 3D microstructural analysis with the same electrode and to compare the reaction distribution directly observed by XAS and that calculated by the ALS model while taking the electrode microstructures into account. To quantitatively investigate the influence of the electrode material on the reaction distribution, it would be useful to perform operando micro XAS measurements using model electrodes in which the electrode microstructure and geometry are well-defined. Both of these investigations are now in progress in our group, and we will report the results elsewhere in the near future.

The direct evaluation of the reaction distribution and electrochemically active area in a porous $La_{0.6}Sr_{0.4}CoO_{3-\delta}$ electrode near the interface with a $Ce_{0.9}Gd_{0.1}O_{1.95}$ electrolyte was successfully accomplished by using operando high-temperature electrochemical micro XAS measurements. The characteristic length of the electrochemically active area was evaluated as approximately 1 μm from the electrode−electrolyte interface under a constant cathodic overpotential of 140 mV at 873 K and 10^{-2} bar of $P(O_2)$. The results obtained in this work demonstrated that the electrochemical reaction proceeds inhomogeneously in a porous SOFC electrode, and only part of the electrode within several micrometers of the electrode−electrolyte interface serves as the reaction sites even when a mixed ionic and electronic conductor is used as an electrode material. Such information about the reaction distribution is essential for the design and optimization of the material and microstructure for high-performance MIEC SOFC electrodes. Moreover, the methodology for interfacial analysis developed in this work can be a general tool, which is applicable to investigate the inhomogeneous reaction and its distribution not only in SOFC but also for various devices, such as other types of fuel cells, electrolysis cells, and even batteries, including all-solid-state lithium ion batteries.

EXPERIMENTAL SECTION

Sample Preparation. A three-terminal electrochemical cell was fabricated with a dense $Ce_{0.9}Gd_{0.1}O_{1.95}$ electrolyte cube. A schematic illustration of the prepared cell is presented in Figure 1. $La_{0.6}Sr_{0.4}CoO_{3-\delta}$ powder was screen-printed on the sintered compact of $Ce_{0.9}Gd_{0.1}O_{1.95}$ with an organic solvent (TMS-1, Tanaka Holdings Co., Ltd.) and fired at 1273 K for 6 h. Detailed procedures for the synthesis of $Ce_{0.9}Gd_{0.1}O_{1.95}$ and $La_{0.6}Sr_{0.4}CoO_{3-\delta}$ are provided in the Supporting Information. The obtained $Ce_{0.9}Gd_{0.1}O_{1.95}$ and $La_{0.6}Sr_{0.4}CoO_{3-\delta}$ powders were confirmed as single-phase fluorite and perovskite, respectively (see Figures S1 and S2). The thickness of the prepared cathode was about 50 μm, as shown in the cross-sectional SEM image in Figure 1. From the SEM observation, it was estimated that the particle size and porosity of the electrode were approximately 0.5 μm and 0.5, respectively. A porous Pt (TR-7907, Tanaka Holdings Co., Ltd.) was put on the back and lateral sides of the electrolyte cube as a counter electrode and a reference electrode, respectively.

Operando XAS Measurement. Operando micro XAS measurements were performed at beamline BL37XU, SPring-8, Japan Synchrotron Radiation Research Institute (JASRI). In this study, the incident X-ray beam from the synchrotron radiation was focused onto a 0.5 μm × 0.8 μm area using a Kirkpatrick-Baez mirror. The prepared electrochemical cell was mounted atop a Pt−Ir electric furnace in the sample holder for operando XAS measurements. The atmospheric $P(O_2)$ around the electrochemical cell was controlled by flowing a mixture of O_2 and He gases, while ensuring the sufficient penetration of incident and fluorescence X-rays to and from the sample, respectively. $P(O_2)$ in ambient atmosphere was controlled in the range of $1-10^{-3}$ bar. The temperature was kept constant at 873 K. All electrochemical measurements were performed with a three-terminal configuration. Before operando XAS measurements, AC EIS measurements was carried out under an open circuit with 10 mV of amplitude in the frequency range between 100 kHz and 100 mHz to confirm the proper operation of the cell and to evaluate the ohmic resistance of the electrolyte. During operando micro XAS measurements, the electrode was cathodically polarized by applying a constant DC bias with a potentiostat/galvanostat (VersaSTAT3, AMETEK, Inc.). The voltage and current responses during the polarization are presented in Figure S3. The cathodic overpotential was calculated by subtracting the *IR* drop from the applied cathodic bias. The *IR* drop was estimated from the ohmic resistance of the electrolyte by EIS measurements and from the current observed during DC polarization.

ASSOCIATED CONTENT

Supporting Information

The Supporting Information is available free of charge at https://pubs.acs.org/doi/10.1021/acs.jpclett.5c02422.

Additional details and notes on synthesis and phase identification of materials and polarization behavior during the operando XAS measurements (PDF)

AUTHOR INFORMATION

Corresponding Author

Koji Amezawa − *Institute of Multidisciplinary Research for Advanced Materials (IMRAM), Tohoku University, Sendai 980-8577, Japan;* orcid.org/0000-0002-3430-6927; Email: koji.amezawa.b3@tohoku.ac.jp

Authors

Yoshinobu Fujimaki − *Institute of Multidisciplinary Research for Advanced Materials (IMRAM), Tohoku University, Sendai 980-8577, Japan*

Takashi Nakamura − *Institute of Multidisciplinary Research for Advanced Materials (IMRAM), Tohoku University, Sendai 980-8577, Japan;* Present Address: Institute of Materials and Systems for Sustainability, Nagoya University, Furo-cho, Chikusa, Nagoya 464-8601, Japan; orcid.org/0000-0001-5461-9958

Yuta Kimura − *Institute of Multidisciplinary Research for Advanced Materials (IMRAM), Tohoku University, Sendai 980-8577, Japan;* orcid.org/0000-0002-3525-1366

Kiyofumi Nitta − *Japan Synchrotron Radiation Research Institute (JASRI), Sayo-gun, Hyogo 679-5198, Japan*

https://doi.org/10.1021/acs.jpclett.5c02422
J. Phys. Chem. Lett. 2025, 16, 9599−9605

Oki Sekizawa − *Japan Synchrotron Radiation Research Institute (JASRI), Sayo-gun, Hyogo 679-5198, Japan*
Yasuko Terada − *Japan Synchrotron Radiation Research Institute (JASRI), Sayo-gun, Hyogo 679-5198, Japan*
Keiji Yashiro − *Graduate School of Environmental Studies, Tohoku University, Sendai 980-8579, Japan;* Present Address: Faculty of Materials for Energy, Shimane University, 1060 Nishikawatsu-cho, Matue-shi, Shimane 690-8504, Japan.
Tatsuya Kawada − *Graduate School of Environmental Studies, Tohoku University, Sendai 980-8579, Japan*

Complete contact information is available at: https://pubs.acs.org/10.1021/acs.jpclett.5c02422

Author Contributions

K.A. conceived and designed the research and performed the operando XAS measurements. Y.F. fabricated and characterized the specimen and performed the operando XAS measurements. Y.K., K.N., O.S., and Y.T. assisted with the operando XAS measurements. K.Y. assisted with the fabrication of the specimen. Y.F., K.A., T.N., and T.K. analyzed the experimental results. K.A. and Y.F. wrote the manuscript with comments from all of the authors.

Notes

The authors declare no competing financial interest.

■ ACKNOWLEDGMENTS

This work was supported by the Japan Society for the Promotion of Science (JSPS) (18H02067 and 21H02036) and the New Energy and Industrial Technology Development Organization (NEDO) (JPNP20003), Japan. Operando micro XAS measurements were performed at SPring-8, Japan (2018A1383, 2018B1375, 2020A0728, 2020A1445, 2021A1375, 2021B1464, and 2022A1429).

■ REFERENCES

(1) Minh, N. Q. Solid oxide fuel cell technology−features and applications. *Solid State Ionics* **2004**, *174*, 271−277.
(2) He, S.; Zou, Y.; Chen, K.; Jiang, S. P. A critical review of key materials and issues in solid oxide cells. *Interdisciplinary Materials* **2023**, *2*, 111−136.
(3) Yatoo, M. A.; Habib, F.; Malik, A. H.; Qazi, M. J.; Ahmad, S.; Ganayee, M. A.; Ahmad, Z. Solid-oxide fuel cells: A critical review of materials for cell components. *MRS Commun.* **2023**, *13*, 378−384.
(4) Xu, Q.; Guo, Z.; Xia, L.; He, Q.; Li, Z.; Temitope Bello, I.; Zheng, K.; Ni, M. A comprehensive review of solid oxide fuel cells operating on various promising alternative fuels. *Energy Convers. Manage.* **2022**, *253*, 115175.
(5) Adler, S. B.; Lane, J. A.; Steele, B. C. H. Electrode kinetics of porous mixed-conducting oxygen electrodes. *J. Electrochem. Soc.* **1996**, *143*, 3554−3564.
(6) Adler, S. B. Mechanism and kinetics of oxygen reduction on porous $La_{1-x}Sr_xCoO_{3-\delta}$ electrodes. *Solid State Ionics* **1998**, *111*, 125−134.
(7) Adler, S. B. Limitations of charge-transfer models for mixed-conducting oxygen electrodes. *Solid State Ionics* **2000**, *135*, 603−612.
(8) Adler, S. B. Factors governing oxygen reduction in solid oxide fuel cell cathodes. *Chem. Rev.* **2004**, *104*, 4791−4843.
(9) Lu, Y.; Kreller, C.; Adler, S. B. Measurement and modeling of the impedance characteristics of porous $La_{1-x}Sr_xCoO_{3-\delta}$ electrodes. *J. Electrochem. Soc.* **2009**, *156*, B513−525.
(10) Rüger, B.; Joos, J.; Carraro, T.; Weber, A.; Ivers-Tiffée, E. 3D electrode microstructure reconstruction and modelling. *ECS Trans.* **2009**, *25*, 1211−1220.
(11) Joos, J.; Carraro, T.; Weber, A.; Ivers-Tiffée, E. Reconstruction of porous electrodes by FIB/SEM for detailed microstructure modeling. *J. Power Sources* **2011**, *196*, 7302−7307.
(12) Carraro, T.; Joos, J.; Rüger, B.; Weber, A.; Ivers-Tiffée, E. 3D finite element model for reconstructed mixed-conducting cathodes: II. Parameter sensitivity analysis. *Electrochim. Acta* **2012**, *77*, 309−314.
(13) Carraro, T.; Joos, J.; Rüger, B.; Weber, A.; Ivers-Tiffée, E. 3D finite element model for reconstructed mixed-conducting cathodes: I. Performance quantification. *Electrochim. Acta* **2012**, *77*, 315−323.
(14) Joos, J.; Ender, M.; Carraro, T.; Weber, A.; Ivers-Tiffée, E. Representative volume element size for accurate solid oxide fuel cell cathode reconstructions from focused ion beam tomography data. *Electrochim. Acta* **2012**, *82*, 268−276.
(15) Matsuzaki, K.; Shikazono, N.; Kasagi, N. Three-dimensional numerical analysis of mixed ionic and electronic conducting cathode reconstructed by focused ion beam scanning electron microscope. *J. Power Sources* **2011**, *196*, 3073−3082.
(16) Szemer, M.; Buchaniec, S.; Prokop, T.; Brus, G. Topology-informed machine learning for efficient prediction of solid oxide fuel cell electrode polarization. *Energy and AI* **2025**, *20*, 100495.
(17) Orikasa, Y.; Ina, T.; Nakao, T.; Mineshige, A.; Amezawa, K.; Oishi, M.; Arai, H.; Ogumi, Z.; Uchimoto, Y. X-ray absorption spectroscopic study on $La_{0.6}Sr_{0.4}CoO_{3-\delta}$ cathode materials related with oxygen vacancy formation. *J. Phys. Chem. C* **2011**, *115*, 16433−16438.
(18) Amezawa, K.; Orikasa, Y.; Ina, T.; Unemoto, A.; Sase, M.; Watanabe, H.; Fukutsuka, T.; Kawada, T.; Terada, Y.; Uchimoto, Y. Electronic and local structures of $La_{1-x}Sr_xCoO_{3-\delta}$ studied by in-situ micro XAS measurements. *ECS Trans.* **2008**, *13*, 161−164.
(19) Tsuji, Y.; Amezawa, K.; Nakao, T.; Ina, T.; Kawada, T.; Yamamoto, K.; Uchimoto, Y.; Orikasa, Y. Investigation of cathodic reaction mechanism in solid oxide fuel cells by operando X-ray absorption spectroscopy. *Electrochemistry* **2020**, *88*, 560−565.
(20) Kawada, T.; Suzuki, J.; Sase, M.; Kaimai, A.; Yashiro, K.; Nigara, Y.; Mizusaki, J.; Kawamura, K.; Yugami, H. Determination of oxygen vacancy concentration in a thin film of $La_{0.6}Sr_{0.4}CoO_{3-\delta}$ by an electrochemical method. *J. Electrochem. Soc.* **2002**, *149*, E252−259.
(21) Sase, M.; Suzuki, J.; Yashiro, K.; Otake, T.; Kaimai, A.; Kawada, T.; Mizusaki, J.; Yugami, H. Electrode reaction and microstructure of $La_{0.6}Sr_{0.4}CoO_{3-\delta}$ thin films. *Solid State Ionics* **2006**, *177*, 1961−1964.
(22) Amezawa, K.; Ina, T.; Orikasa, Y.; Unemoto, A.; Watanabe, H.; Iguchi, F.; Terada, Y.; Fukutsuka, T.; Kawada, T.; Yugami, H.; Uchimoto, Y. Investigation on oxygen potential distribution in a ZrO_2-based solid electrolyte by using in-situ micro XAS technique. *ECS Trans.* **2009**, *25*, 345−348.
(23) Boukamp, B. A.; Bouwmeester, H. J. M. Interpretation of the Gerischer impedance in solid state ionics. *Solid State Ionics* **2003**, *157*, 29−33.
(24) Raistrick, I. D. In *Impedance Spectroscopy*; Macdonald, J. R., Ed.; Wiley: New York, 1987.